

Surrogate gradients for analog neuromorphic computing

B. Cramer^{a,1,2}, S. Billaudelle^{a,1,2},
S. Kanya^a, A. Leibfried^a, A. Grübl^a, V. Karasenko^a, C. Pehle^a, K. Schreiber^a, Y. Stradmann^a, J. Weis^a,
J. Schemmel^a, and F. Zenke^{b,2}

^aKirchhoff-Institute for Physics, Heidelberg University, Germany

^bFriedrich Miescher Institute for Biomedical Research, Basel, Switzerland

¹Authors with equal contribution

²Corresponding authors (benjamin.cramer,sebastian.billaudelle@kip.uni-heidelberg.de,friedemann.zenke@fmi.ch)

November 6, 2021

To rapidly process temporal information at a low metabolic cost, biological neurons integrate inputs as an analog sum but communicate with spikes, binary events in time. Analog neuromorphic hardware uses the same principles to emulate spiking neural networks with exceptional energy-efficiency. Nevertheless, emulating high-performing spiking networks on such hardware remains a significant challenge due to device-mismatch and the lack of efficient training algorithms. Here, we introduce a general in-the-loop learning framework that resolves these issues. Using the BrainScales-2 neuromorphic system, we show that learning self-corrects for device mismatch resulting in competitive spiking network performance on vision and speech benchmarks. Our networks display sparse spiking activity with, on average, far less than one spike per hidden neuron, perform inference at rates of up to 85 k frames/second, and consume less than 200 mW. In summary, our work sets several new benchmarks for low-energy spiking network processing on analog neuromorphic substrates and constitutes an important step toward on-chip learning.

Introduction

In recent years, deep artificial neural networks (ANNs) have surpassed human-level performance on several complex tasks (Mnih et al., 2013; Silver et al., 2017; Brown et al., 2020). The human brain, however, remains unchallenged in terms of its energy-efficiency and fault tolerance. A fundamental property underlying these capabilities is spatiotemporal sparseness (Sterling and Laughlin, 2015), which is directly linked to the way how biological spiking neural networks (SNNs) process and exchange information. Spiking neurons receive and integrate inputs on their analog membrane potentials and, upon reaching the firing threshold, emit action potentials, or spikes. These binary events propagate asynchronously through the SNN and ultimately received by other neurons.

Neuromorphic engineering attempts to mirror the power efficiency and robustness of the brain by replicating its key ar-

chitectural properties (Mahowald and Douglas, 1991; Schemmel et al., 2010; Indiveri et al., 2011; Chicca et al., 2014; Merolla et al., 2014; Benjamin et al., 2014; Furber, 2016; Boahen, 2017; Davies et al., 2018; Roy et al., 2019). One differentiates between fully digital, analog, and mixed-signal systems. While digital systems simulate the analog membrane potentials of spiking neurons, analog and mixed-signal solutions *emulate* neuronal state dynamics by representing them as physical voltages and currents evolving in continuous time.

To solve computational tasks, the SNNs on these devices need to be trained, which requires solving several challenges simultaneously. First, one has to overcome the binary nature of spikes, which impedes vanilla gradient-descent (Bengio et al., 2013; Courbariaux et al., 2016; Neftci et al., 2019), while simultaneously capitalizing on sparse activity and spike timing. And one has to do it in a robust way that takes into account hardware imperfections inevitably tied to the manufacturing of analog hardware.

In this article, we tackle all of the above challenges. Extending previous work on surrogate gradients, we developed a general in-the-loop (ITL) training framework and applied it to the mixed-signal BrainScaleS-2 single-chip system. We demonstrate that our approach solves several challenging benchmark problems requiring precisely timed spikes instead of firing rates. We further show that the resulting trained recurrent SNNs perform at comparable accuracy levels as corresponding software simulations and allow for ultra-low latency inference due to the accelerated neuromorphic substrate. Crucially, we show that ITL training is self-calibrating in that it automatically corrects for device mismatch and therefore abolishes the need for tedious hardware calibration.

Neuromorphic spiking neural network model

The analog BrainScaleS-2 single chip system (Fig. 1A) features 512 analog neuron circuits emulating the adaptive exponential leaky integrate-and-fire (AdEx) model, a superset of the leaky

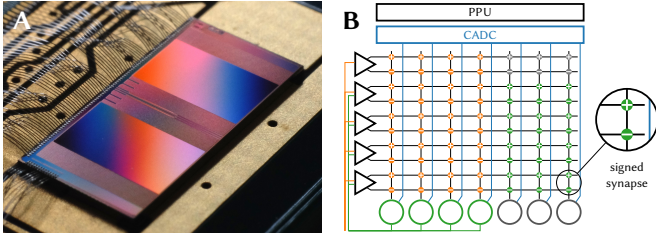


Figure 1: The mixed-signal BrainScaleS-2 ASIC. (A) Close-up of the BrainScaleS-2 ASIC. (B) Implementation of a multi-layer network on the analog neuromorphic core. Input spike trains are injected via synapse drivers (triangles) and relayed to the hidden layer neurons (green circles) via the synapse array. Spikes in the hidden layer are routed on-chip to the output units (gray circles). Each connection is represented by a pair of excitatory and inhibitory hardware synapses, which holds a signed weight value. The analog membrane potentials are read out via the column-parallel analog-to-digital converter (CADC) and further processed by the plasticity processing unit (PPU).

integrate-and-fire (LIF) equation

$$C \frac{dV}{dt} = -g_l (V - E_l) + I, \quad (1)$$

which describes the evolution of the membrane potential V . It is explicitly represented on chip as an analog voltage measured across a capacitor and evolves continuously in time (Fig. 1B). The conductance g_l pulls the membrane towards the leak potential E_l , resulting in an exponential decay with time constant $\tau_{\text{mem}} \equiv C/g_l$. Due to the substrate’s small intrinsic capacitances and comparatively large g_l , the dynamics of the spiking neurons implemented on the BrainScaleS-2 application-specific integrated circuit (ASIC) evolve 10^3 times faster than biological neurons. When the potential crosses the firing threshold ϑ , the membrane is reset and an outgoing spike is emitted. For fine-grained control, all parameters such as reference potentials and time constants can be individually configured and tuned on a per neuron basis (Tab. 3).

Each neuron circuit receives stimuli via a column of 256 synapses, each of which has a weight with 6 bit resolution. The resulting postsynaptic currents I , which are integrated on the membrane capacitor, follow an exponential time course similar to the membrane itself. In the synaptic connectivity matrix, the sign of a synapse is determined as a row-wise property. To allow for a continuous transition between positive and negative weights during training, we represent each connection through two merged synapse circuits of opposing signs (Fig. 1C). Spikes are propagated by an on-chip event routing system, which allows to connect external stimuli as well as the neuron circuits in feed-forward and recurrent topologies.

Surrogate gradient learning with analog hardware in the loop

We developed a general learning framework to optimize recurrent and multi-layer networks of such analog neurons through gradient descent. It operates on arbitrary differentiable loss functions and in particular allows to exploit spike-timing-based coding. For this purpose, we constructed a computation graph which closely follows the dynamics of the analog circuits. To

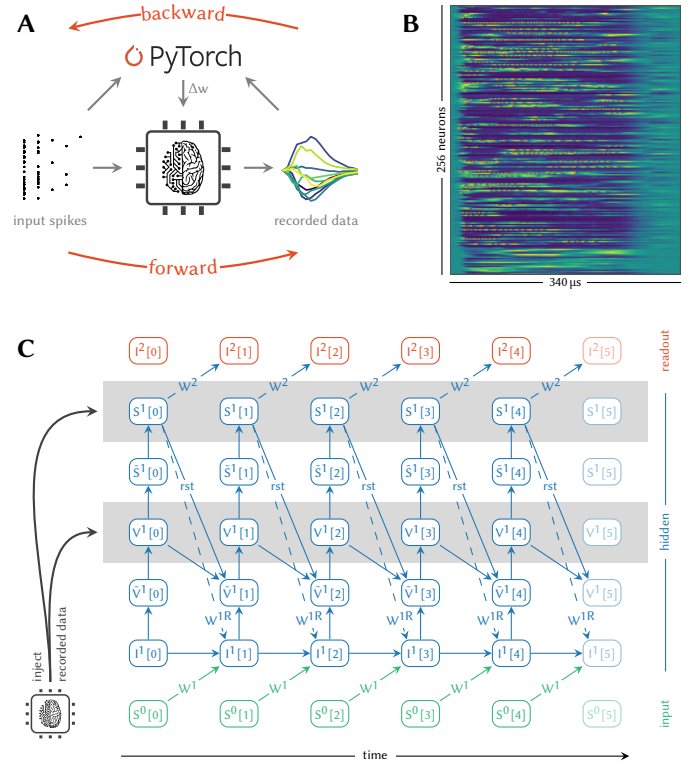


Figure 2: Surrogate gradient learning on BrainScaleS-2. (A) Illustration of our ITL training scheme. The forward pass is emulated on the BrainScaleS-2 ASIC. Observables from the neuromorphic substrate as well as the input spike trains are processed on a conventional computer to perform the backward pass. The calculated weight updates are then written to the neuromorphic system. (B) Parallel recording of analog traces and spikes from 256 neurons via the CADC. (C) The differentiable computation graph results from the integration of LIF dynamics. The time dimension is unrolled from left to right and information flows from bottom to top within an integration step. Synaptic currents are derived from the previous layer’s spikes and potential recurrent connections, multiplied by the respective weights ($W^{(R)}$). Stimuli are integrated on the neurons’ membranes (V) which trigger spikes (S) upon crossing their thresholds. These observables are continuously synchronized with data recorded from the hardware. Spikes as well as reset signals (rst) are propagated to the next time step, which also factors in the decay of currents and potentials.

overcome the critical points associated with the insertion and deletion of spikes, we furthermore rely on surrogate gradients (Zenke and Ganguli, 2018; Neftci, 2018). The neuromorphic SNN is effectively made differentiable and its gradients can be estimated through auto-differentiation (Paszke et al., 2019). Specifically, the analog neuromorphic computation represents the forward pass, whereas the backward pass is performed on a host computer via backpropagation through time (BPTT) (Fig. 1A).

Recording spikes and analog membrane traces. To retrieve inference results and further optimize a network, knowledge of the neuromorphic system’s state is required. Typically, most platforms support the read out of digitized spike times, which can hence be directly incorporated into weight update calculations. Surrogate gradient learning, however, also involves the neurons’ membrane potentials. These internal states are represented as physical voltages and thus not readily avail-

able for numerical computation on the host computer. Digitization is challenging due to the inherent parallelism of analog neuromorphic substrates which is further emphasized in accelerated systems.

BrainScaleS-2 solves this problem by incorporating column-parallel analog-to-digital converters (CADCs) to simultaneously digitize the membrane potentials of all neurons (Fig. 1B). We furthermore use the embedded plasticity processing units (PPUs) (Friedmann et al., 2017) of the ASIC to trigger the ADC conversions, ensuring higher and more stable sampling rates when compared to a host-based readout. The PPUs furthermore enable the implementation of a fast inference mode, where only crucial classification results are transmitted to the host machine. Including the transfer of data to an external memory region we reach a sample rate of approximately $0.6 \text{ MSample s}^{-1}$, which corresponds to a sampling interval of $1.7 \mu\text{s}$. For 256 neurons, this yields a data rate of 1.2 Gbit s^{-1} . The traces are asynchronously read back by the host machine after completion of an input pattern or batch. In this setup, the maximum duration of recording is limited by the available memory and batch size.

A computation graph for analog circuits. Despite our knowledge of hardware spike times and membrane potentials, these data do not allow to calculate their exact partial derivatives to directly perform weight update calculations through BPTT. To instead gather estimates of the gradients, we hence construct a differentiable computation graph, which merges a numerical model of the neuromorphic system’s dynamics with the acquired, actual data (Fig. 1C). For the sake of simplicity, the model is formulated on a regular grid of time step Δt which is aligned with the sampling period of the recorded membrane potentials. At the same time, the spike trains, which arrive from the neuromorphic substrate with a much higher resolution, are binned to the same interval. Depending on the coding scheme and network topology, an increased resolution can be beneficial, which allows the computation graph to better capture causal relations between spike times. In this case, an interpolation of the acquired membrane traces can be performed.

To construct the model, we rely on the LIF equation (Eq. 1), which we integrate using a forward-Euler method. The membrane evolution can be estimated recursively by taking into account its temporal decay and the calculated synaptic currents $\tilde{I}[t]$, which in turn are based on the presynaptic spikes $\tilde{S}_j[t]$ of neuron j :

$$\tilde{V}[t + 1] = \tilde{V}[t] \cdot e^{-\Delta t/\tau_{\text{mem}}} + \tilde{I}[t], \quad (2)$$

$$\tilde{I}[t + 1] = \tilde{I}[t] \cdot e^{-\Delta t/\tau_{\text{syn}}} + \sum_j W_j \tilde{S}_j[t]. \quad (3)$$

Here, Eq. 3 can be augmented by an additional term to encompass recurrence. All of these variables represent modelled states, which is indicated by the tilde ($\tilde{\cdot}$). However, this simple model does not capture higher-order effects in the analog circuits and \tilde{V} and \tilde{S} can deviate from the actual values V and S as sampled from the hardware. Therefore it is desirable to use the *actual* recordings whenever possible and only resort to the model to calculate their derivatives. To achieve this, we introduce an auxiliary identity function $f(x, \tilde{x}) \equiv x$ and define surrogate derivatives $\partial f/\partial x = 0$ and $\partial f/\partial \tilde{x} = 1$. Eq. 2 can now

be modified to

$$\tilde{V}[t + 1] = f(V[t + 1], \tilde{V}[t] \cdot e^{-\Delta t/\tau_{\text{m}}} + \tilde{I}[t]). \quad (4)$$

A similar approach is taken for spikes by defining $\tilde{S}_j[t](S_j[t], \tilde{V}_j[t]) \equiv S_j[t]$ with associated surrogate derivatives

$$\frac{\partial \tilde{S}_j[t]}{\partial S_j[t]} = 0, \quad \frac{\partial \tilde{S}_j[t]}{\partial \tilde{V}_j[t]} = (\beta \cdot |\tilde{V}_j[t] - \vartheta|)^{-2}, \quad (5)$$

where β describes the steepness of the surrogate gradient (Zenke and Ganguli, 2018).

When performing the backward pass and to this end calculating $\partial \mathcal{L}/\partial \theta = \dots \partial \tilde{S}/\partial \tilde{V} \cdot \partial \tilde{V}/\partial \theta$, the sampled values for the membrane potential are used whenever an expression containing \tilde{V} is evaluated, e.g. $\partial \tilde{S}/\partial \tilde{V}$. The model of the membrane, however, is used to determine further derivatives that occur in $\partial \tilde{V}/\partial \theta$.

Flexible choice of a loss function. The suggested framework allows to operate on any differentiable loss that can be formulated on the data acquired from the neuromorphic system. This encompasses spike-time-based loss functions (Mostafa, 2018; Göltz et al., 2019), but depending on the task it can be beneficial to make use of non-spiking leaky integrators for the readout layer. These can be implemented simply by disabling the neurons’ spiking mechanism. In this case, the network’s response to a stimulus is directly encoded in the evolution of the last layer’s membrane potentials $V_i^L[t]$. When considering e.g. their maximum deflection from the resting state, a max-over-time loss

$$\mathcal{L} = \text{NLL} \left(\text{softmax} \left(\max_t V_i^L[t] \right), y^* \right) \quad (6)$$

can be employed, which involves the negative log-likelihood NLL and the true labels y^* (Cramer et al., 2020). Similarly, a sum-over-time can be obtained by replacing the max-operator by a sum.

The task-specific loss can be augmented by regularization functions to e.g. improve a model’s ability to generalize on unseen data or to better utilize the available dynamic range of activations or model parameters. Such terms can also be directly tailored to shape the activity of an SNN and result in firing patterns which are sparse in space and time. This is of particular interest in the field of neuromorphic engineering, where the overall power consumption often correlates with the spike count.

Results

We applied our in-the-loop framework to train the analog neuromorphic BrainScaleS-2 system on a series of tasks. The data sets were chosen to exhibit widely different time scales and suggest both feed-forward as well as recurrent network topologies.

First, we trained a feed-forward network consisting of a single hidden layer with 246 neurons on the MNIST dataset (LeCun et al., 1998). To accommodate the data to a fan-in of 256 inputs, we reduced the original 28×28 images to 16×16 pixels, which were then converted into a spike-latency code (cf. Materials and methods). The network was optimized using the

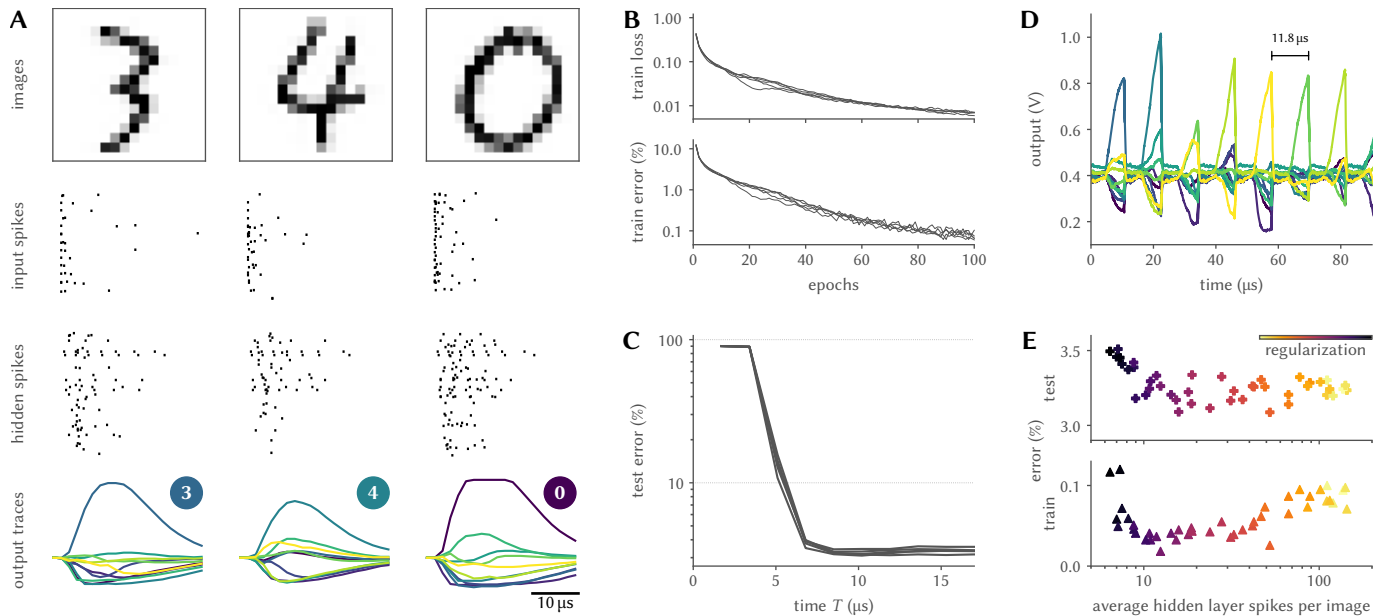


Figure 3: Classification of the MNIST dataset. (A) Three snapshots of the SNN activity, consisting of the downscaled 16×16 input images (top), spike raster of both the input spike trains and hidden layer activity (middle), and readout neuron traces (bottom). The latter show a clear separation, and hence a correct classification of the presented images. (B) Loss and accuracy over the course of 100 training epochs for five initial conditions. (C) The time to decision is consistently below $10 \mu\text{s}$. Here, the classification latency was determined by iteratively re-evaluating the max-over-time for output traces (see panel A) restricted to a limited interval $[0, T]$. (D) This low latency allowed to inject an image every $11.8 \mu\text{s}$, corresponding to more than 85 k classifications per second. This was achieved by artificially resetting the state of the neuromorphic network in between samples. (E) The neuromorphic system can be trained to perform classification with sparse activity. When sweeping the regularization strength, a state of high performance was evidenced over more than an order of magnitude of hidden layer spike counts.

Adam optimizer (Kingma and Ba, 2014) operating on a max-over-time loss, augmented by regularization terms. It is noteworthy, that the surrogate-gradient approach allowed to train the network starting from a quiescent hidden layer, even without a regularization term enforcing network activity.

During training, the neuromorphic substrate learned to correctly encode the samples’ class memberships through the maximally responsive output units (Fig. 3A,B). The inhibition of incorrect units, interestingly, did not explicitly result from the loss function (Eq. 6) but rather emerged as a byproduct. After 100 epochs, the model was able to almost perfectly fit the training samples. On the held out test data, the trained network achieved an overall accuracy of $(96.7 \pm 0.1) \%$ (Table 1). We were able to reduce overfitting by data augmentation, specifically by applying random rotations of up to 15° to the presented images. Dropout regularization similarly improved test performance. A combination of both resulted in a best-effort accuracy of $(97.6 \pm 0.0) \%$ on BrainScaleS-2.

When training the same SNN purely in software, it reached $(97.5 \pm 0.1) \%$ on the test data. As a baseline, we also trained an equivalently sized ANN with rectified linear units (ReLU) on the 16×16 pixel version of MNIST: The network reached an accuracy of $(98.1 \pm 0.1) \%$. Dropout as well as augmentation again improved upon these numbers resulting in a best-effort performance of $(98.7 \pm 0.1) \%$.

Low-latency neuromorphic computation. The employed spike latency-input coding suggests short decision times. We hence analyzed the network’s inference latency by artificially restricting the readout layer’s membrane traces (cf. Fig. 3A) to

time intervals $[0, T]$. Fig. 3C shows how peak accuracy is already reached within $8 \mu\text{s}$ after the first input spike.

We exploited this low classification latency to implement a fast inference mode. For this purpose, we added an artificial reset of all units on the neuromorphic system. $10 \mu\text{s}$ after inserting the first input spike, we triggered a silent reset of the analog membrane circuits and at the same time clamped all synaptic currents to their baselines (Fig. 3D). This allowed us to inject images with a separation of only $11.8 \mu\text{s}$, corresponding to a throughput of 85 k images per second.

We furthermore studied the system’s power consumption. For the full ASIC emulating the trained SNN, we measured approximately 200 mW. This figure includes the current draw from the analog neuromorphic core, the plasticity processors, and all surrounding periphery. The overall figure was dominated by the idle power spent on clock generation and distribution as well as the communication links to and from the ASIC. Combining this measurement with above’s throughput yields an energy consumption of only $2.4 \mu\text{J}$ per classified image.

Efficiency through sparse spiking activity. One of the most remarkable phenomena in neurobiology is sparse spiking activity (Sterling and Laughlin, 2015). To attain similar behavior on the BrainScaleS-2 system, we augmented the training loss by an adjustable sparseness penalty

$$\mathcal{L}_{\text{reg}} = \rho_b \frac{1}{N_H} \sum_{i=1}^{N_H} \left(\sum_t S_i^H[t] \right)^2,$$

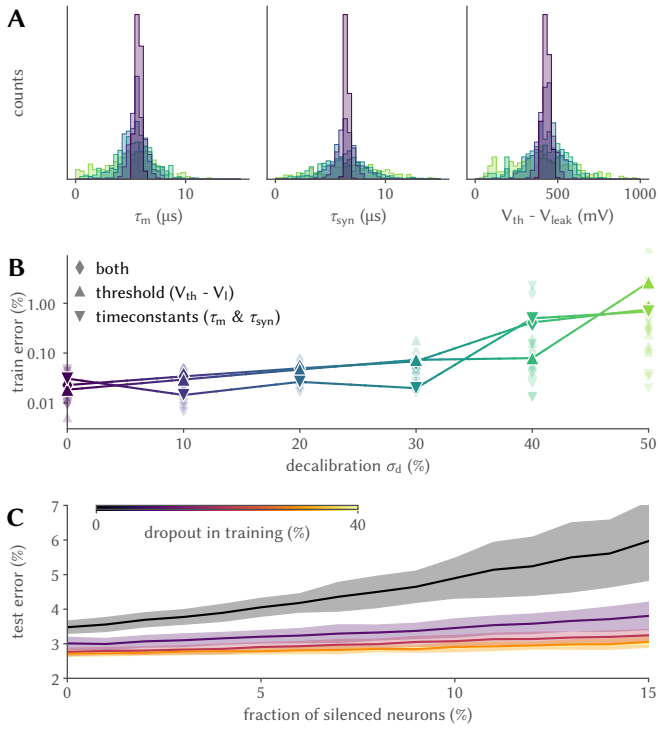


Figure 4: Robust training and classification on inhomogeneous substrates. (A) Distribution of measured neuronal parameters for various degrees of decalibration in the range of 0% to 50%. For this purpose, the analog circuits were deliberately detuned towards individual target values drawn from normal distributions of variable widths. (B) Despite assuming homogeneously behaving circuits in the computation graph, ITL training widely compensated the fixed-pattern deviations shown in panel A. For configurations with extreme mismatch, some networks suffered from dysfunctional states (e.g. leak-over-threshold). (C) When incorporating dropout regularization during training, networks become widely resilient to failure of hidden neurons.

with the strength parameter ρ_b , the hidden layer size N_H , and the corresponding hidden layer spike trains S_i^H . We trained the above feed-forward SNNs for a range of different values ρ_b and measured both their accuracy and average hidden layer spike counts. All resulting network configurations were able to almost fit the training data (Fig. 3E). More importantly, they reached a constant test accuracy of approximately 96.5% for activations down to 10 hidden layer spikes per image. Even with only 6 spikes, only a slight decrease in performance was observed. At these low spike counts, the networks operated in a regime far from the rate coding limit and hence relied on individual spikes and their timing. This can be of particular interest for neuromorphic devices, where power consumption directly correlates with network activity.

Self-calibration through ITL training. The above results were obtained with a calibrated BrainScaleS-2 ASIC, which resulted in a close alignment between the emulated dynamics and the computation graph. Still, a certain degree of parameter mismatch between neuronal units had to be accepted (cf. Fig. 4A). To investigate the limits of the presented ITL training scheme, we deliberately detuned the membrane and synaptic time constants as well as the firing threshold. For this pur-

pose, we calibrated each unit to individual target values, which were drawn from normal distributions with the original target as the mean and a variable standard deviation. This defined the decalibration σ_d , given as the standard deviation normalized to the mean. We generated sets of configuration values with σ_d in the range of 0% to 50% (Fig. 4A) for five seeds and three distinct scenarios: First, we individually detuned the time constants and the distance between leak and threshold, respectively. Second, all of these parameters were decalibrated at the same time.

For each of these parameter sets, we trained the SNN on the neuromorphic system but in this process ignored the (deliberately introduced) mismatch when constructing the computation graph. Thereby we assumed ideal dynamics despite of the imperfect emulation. The SNN still reached a high level of performance for a decalibration of up to $\sigma_d = 30\%$. Beyond that point, most configurations continued to yield high accuracy levels. Individual trials, however, suffered from dysfunctional network states induced by leak-over-threshold conditions, reflected in increased errors.

Training for robustness. We furthermore investigated the resilience of trained SNNs to hardware defects occurring after deployment. The latter were simulated by artificially silencing individual units in the hidden layer of the network (Fig. 4C). As expected, performance deteriorated with an increasing fraction of disabled neurons.

Tab. 1 already noted how dropout regularization improved the network’s ability to generalize. Besides boosting the test accuracy, it as a side effect also increased the resilience to neuron failure: For networks trained with a dropout of 40% the test error increased by only 11% when silencing 15% of the hidden layer. In contrast, it grew by 72% when not employing dropout regularization.

Speech recognition with recurrent SNNs. BrainScaleS-2 is not restricted to feed-forward architectures but supports arbitrary topologies, including recurrent networks. When constructing the computation graph for BPTT-based training, the model of synaptic currents (Eq. 3) is then simply augmented by the recurrent contributions.

We trained a network with a recurrent hidden layer to classify the SHD (Cramer et al., 2020) dataset, which consists of spoken digits from »zero« to »nine« in English as well as German, resulting in a total of 20 classes. This dataset appeared natural for benchmarking SNNs – especially with recurrent connectivity – for two reasons: It features an inherent temporal dimension and furthermore provides the samples directly in the form of spike trains, and hence alleviates the need for additional preprocessing and encoding. We reduced the dimensionality of the input by sampling 70 from the original 700 channels (cf. Materials and methods) and injected them into a recurrent hidden layer of 186 neurons. The network was then trained by optimizing a sum-over-time loss (Fig. 5A). To prevent pathological firing activities, we employed a regularization term $\rho_r \cdot \max(0, \sum_{i,t} S_i[t] - \theta_r)^2$ where i and t iterate over the hidden layer units and time steps, respectively. ρ defines the regularization strength and θ_r a threshold.

After 100 epochs, the trained network reached $(96.6 \pm 0.5)\%$ on the training data and $(76.2 \pm 1.3)\%$ on the test set (Fig. 5B,

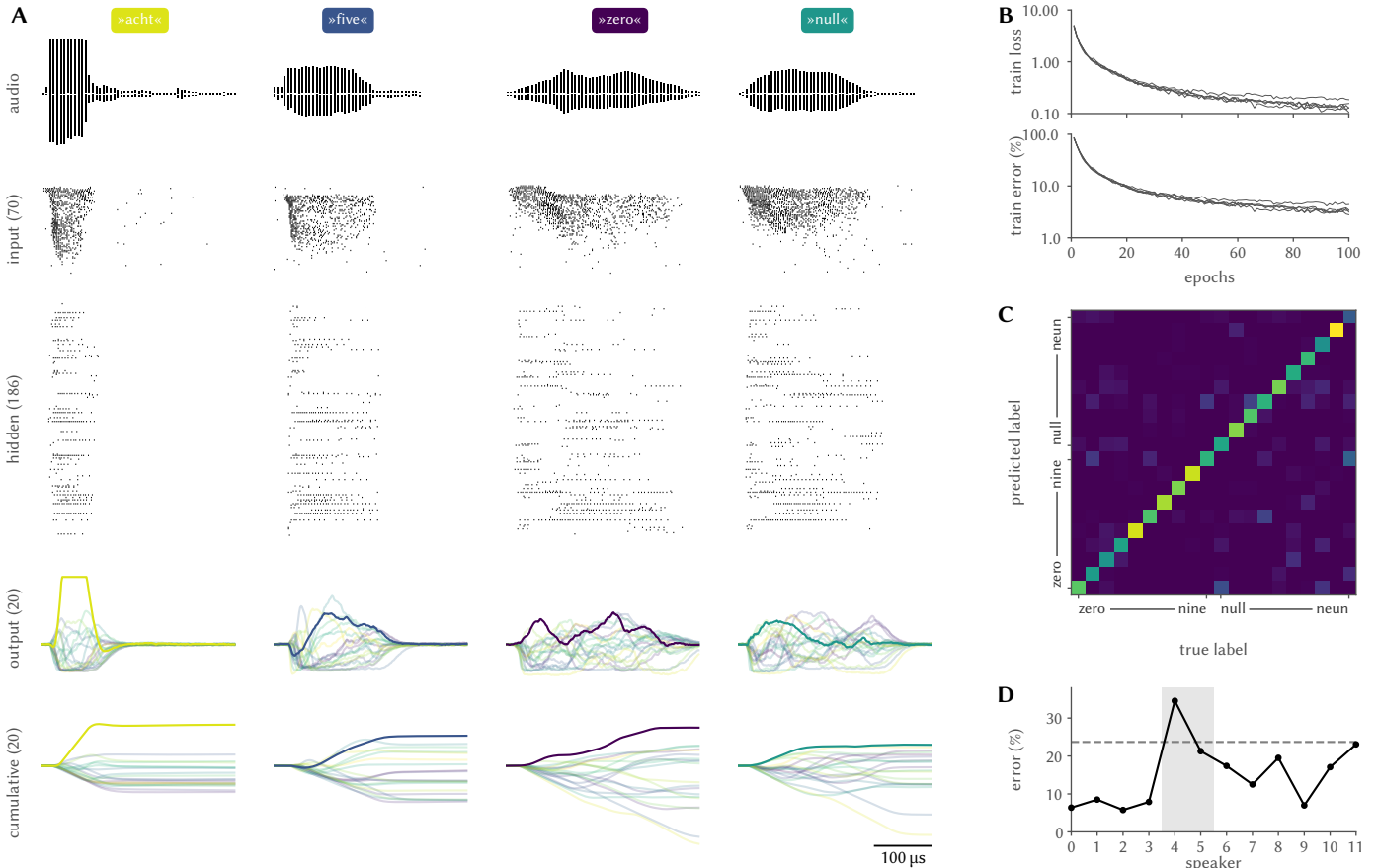


Figure 5: Classification of natural language with recurrent SNNs on BrainScaleS-2. (A) Responses of a recurrent network when presented with samples from the spiking Heidelberg digits (SHD) dataset. The input spike trains, originally derived from recordings of spoken digits (see illustrations), were reduced to 70 stimuli. The network was trained according to a sum-over-time loss based on the output units’ membrane traces. For visualization purposes, we also show their cumulative sums. (B) Over 100 epochs of training, the network developed suitable representations as evidenced by a reduced training loss and error, here shown for five distinct initial conditions. (C) Classification performance varies across the twenty classes, especially since some of them exhibit phonemic similarities (»nine« vs. »neun«). (D) The trained network generalizes well on unseen data from most speakers included in the dataset. The discrepancy between training and overall test error (dashed line) arises from the composition of the dataset: 81 % of the test set’s samples stem from two exclusive speakers (highlighted in gray).

Tab. 1). This discrepancy resulted from the nature of the dataset, which was designed to especially challenge a network’s ability to generalize (Cramer et al., 2020). The two languages included in the dataset exhibit classes with significant phonemic similarity (»nine« vs. »neun«), which are indeed harder to separate by the trained network (Fig. 5C). Most importantly, however, the samples of two of the twelve speakers exclusively occur in the test set, where they constitute 81 % of the data. On these, a higher classification error is observed (Fig. 5D).

Discussion

We have developed a general ITL training method for recurrent and multi-layer SNNs on analog neuromorphic substrates. Specifically, we have used the BrainScales-2 neuromorphic system to emulate the forward pass of an SNN. Recording every analog membrane potential in parallel permitted us to compute surrogate gradients in software for supervised learning. Crucially, our ITL learning framework was self-correcting for device mismatch, thereby essentially abolishing the need for tedious calibration. Using our framework, we trained recur-

Table 1: Comparison of results achieved with networks trained on BrainScaleS-2 and in software as well as an ANN baseline.

dataset	substrate	remarks	accuracy (%)	
			train	test
16×16 MNIST	BSS-2		99.9 ± 0.1	96.6 ± 0.1
	BSS-2	dropout	99.0 ± 0.0	97.3 ± 0.1
	BSS-2	dropout + rotation	96.6 ± 0.1	97.6 ± 0.0
	software		100.0 ± 0.0	97.5 ± 0.1
	ANN	dropout + rotation	100.0 ± 0.0	98.1 ± 0.1
SHD	BSS-2		96.6 ± 0.5	76.2 ± 1.3
	BSS-2	augmentation	90.7 ± 0.5	80.6 ± 1.0
	software		99.3 ± 0.2	70.4 ± 0.8
	software	augmentation	88.3 ± 0.3	76.7 ± 0.8

rent and multi-layer SNNs on SHD, and a spike-latency encoded version of MNIST. In all cases, we achieved classification accuracies comparable to software simulations of equivalent networks and establish new benchmarks for low-latency processing and energy efficiency compared to other neuromorphic platforms. Thereby the intrinsic hardware acceleration factor of BrainScales-2 allowed to classify more than 85 k MNIST im-

ages per second on a power budget of less than 200 mW. To the best of our knowledge, this is the first instance of a recurrent analog neuromorphic SNN trained on a real-world dataset that efficiently used spike-timing for information processing.

In the present article, we have extended surrogate gradient learning to an ITL learning setting, which allowed us to train recurrent and multi-layer SNNs on hardware. This problem was approached from several different angles in the past. For instance, many studies focused on unsupervised learning rules inspired by biology (Tavanaei et al., 2019). However, their success in comparison to supervised learning has remained limited. Supervised learning in deep SNNs requires solving both a spatial and temporal credit assignment problem. To that end, many training strategies attempt to translate the success of gradient-based learning to the realm of SNNs (Pfeiffer and Pfeil, 2018; Neftci et al., 2019). We distinguish between direct and indirect methods. The most successful indirect approach is *network translation* in which one first trains a non-spiking ANN and then translates it into an SNN (Rückauer et al., 2019; Zambrano et al., 2019; Stöckl and Maass, 2020; Büchel et al., 2021). However, the resulting networks typically rely on rate-coding and do not take advantage of spike-timing. Direct training refers to methods that operate on the parameters of the SNN themselves. We further subdivide them into smoothing, firing-time gradient, and surrogate gradient approaches. First, *smoothing approaches* attempt to render the forward model differentiable by either introducing graded spikes (Huh and Sejnowski, 2018) or stochasticity (Ackley et al., 1985; Bengio et al., 2013; Brea et al., 2013; Gardner and Grünig, 2016; Jimenez Rezende and Gerstner, 2014; Guerguiev et al., 2017). However, adding stochasticity typically requires averaging to reduce the variance of the gradient estimates by relying on firing rates or population coding (Hunsberger and Eliasmith, 2015; O’Connor and Welling, 2016; Lee et al., 2016; Neftci et al., 2017; Guerguiev et al., 2017; Payeur et al., 2020). Second, *firing-time gradients* can be adopted in cases in which the neuronal membrane potential (Gütig and Sompolinsky, 2006; Memmesheimer et al., 2014) or firing times can be expressed analytically in closed form (Bohte et al., 2002; Mostafa, 2018; Mozafari et al., 2019; Göltz et al., 2019; Comsa et al., 2020). This method leaves the forward model unchanged and allows to exploit temporal coding but needs additional mechanisms to deal with quiescent neurons or multiple spikes. In multi-layer networks, it has only been demonstrated in conjunction with time-to-first-spike coding schemes. Finally, *surrogate gradient approaches* do not add such constraints while also leaving the forward model unchanged. Instead, they directly apply approximations to the gradients, a notion inspired by work on binary ANNs (Bengio et al., 2013; Courbariaux et al., 2016). Surrogate gradient approaches are surprisingly successful in training SNNs that take advantage of spike-timing (Bohte, 2011; Esser et al., 2016; Zenke and Ganguli, 2018; Shrestha and Orchard, 2018; Bellec et al., 2018; Wozniak et al., 2018; Neftci et al., 2019) without explicitly having to specify a coding strategy. In this article, we reported the first application of surrogate gradients to an analog neuromorphic substrate.

Most existing work on both digital and analog systems typically employed rate-based coding schemes, which often entail higher activity levels and longer latencies. For instance, Schmitt et al. (2017) have used a comparable ITL approach to

train rate-coding SNNs in the analog setting, whereas several other studies were carried out on digital hardware (Chen et al., 2019; Stromatias et al., 2015; Lin et al., 2018; Frenkel et al., 2018) (see Table 2 for a comparison). One notable exception to the rate-based coding scheme is the work of Göltz et al. (2019) which used a spike-timing code using the same BrainScales-2 hardware, but was limited to feed-forward architectures.

Finally, one should note that a detailed quantitative comparison between the different approaches and systems remains challenging. This difficulty is partially due to the lack of suitable metrics and standardized benchmarks (Davies, 2019; Cramer et al., 2020). Especially fair comparisons of the net energy footprint are often involved. For instance, some studies rely entirely on simulation estimates (Yin et al., 2017, 2020), which contrasts with the present work.

In summary, our ITL training framework gives a glimpse of the extensive opportunities that analog SNN hardware offers for energy-efficient ultra-low latency information processing while simultaneously highlighting the importance of training methods that take into account and actively compensate device specific imperfections. ITL training is therefore an intermediate step toward on-chip training which will be ultimately required to reap the full benefits of this emergent technology.

Materials and methods

Software environment Our training framework was based on PyTorch’s auto-differentiation library (Paszke et al., 2019). It furthermore builds upon the BrainScaleS-2 software stack to configure the neuromorphic system and execute the experiments (Müller et al., 2020).

Input coding We scaled the MNIST dataset down to 16×16 pixels by first discarding the two outermost rows and scaling the remaining pixels. The images were then converted to spikes by interpreting the normalized pixel grayscale values x_i as input currents to LIF neurons. Strong enough currents trigger a spike at time $t_i = \tau_{\text{in}} \log x_i / (x_i - \vartheta_{\text{in}})$, where τ_{in} denotes the input units time constant and ϑ_{in} its threshold.

Since the SHD dataset is provided in form of input spike times, a custom conversion was not required. To reduce its dimensionality, we however sampled 70 of the original 700 input units by omitting the first 70 and then selecting every ninth. The time dimension was scaled by a factor of 2000 to reflect the accelerated system’s speedup of 1000 and further shorten the experiment duration. When employing data augmentation, a spike originally originating from input channel i was reassigned to a neighboring channel drawn from $\mathcal{N}(\mu = i, \sigma)$. This augmentation was applied prior to downsampling the inputs.

Initialization We used Kaming’s initialization scheme (He et al., 2015) for both the hidden and label layer weight matrices. Specifically, weights were drawn from a normal distribution with zero mean and a standard deviation of $\hat{\sigma}_w / \sqrt{N_{\text{HL}}}$.

Weight scaling Weight values had to be scaled, rounded, and cropped to the neuromorphic system’s weight resolution of 7 bit signed integers (after merging two 6 bit synapses). The

Table 2: Comparison of MNIST benchmark results across neuromorphic platforms. R/T denotes the use of rate or temporal coding.

platform	architecture	energy	accuracy	rate
SpiNNaker (Stromatias et al., 2015)	784-600-500-10 (R)	3.3 mJ	95.0 %	91
TrueNorth (Esser et al., 2016)	CNNs (R)	108.0 μ J	99.4 %	1 k
Intel (Chen et al., 2019)	784-236-20-10 (T)	17.1 μ J	89.0 %	6.25 k
Intel (Chen et al., 2019)	784-1024-512-10 (T)	112.4 μ J	98.2 %	
Intel (Chen et al., 2019)	784-1024-512-10 (T)	1.7 μ J	97.9 %	
BSS-1 (Schmitt et al., 2017)	100-15-15-5 (R)	7.3 mJ	95.0 %	10 k
this work	256-118-10 (T)	2.4 μ J	97.6 %	85 k

exact scaling resulted from analog bias currents and other technical parameters. Due to the absence of a threshold for the non-spiking label layer, its membrane traces could be scaled arbitrarily.

For the MNIST classification, we adopted a dynamic weight scaling for the output weights by aligning the largest absolute weight value as represented in software to the maximum weight possible on the substrate.

Table 3: Parameters for the neuromorphic substrate and training framework.

parameter	symbol	value (MNIST / SHD)
leak potential	E_l	550 mV
firing threshold	θ	850 mV
membrane time constant	τ_{mem}	6 μ s / 10 μ s
synaptic time constant	τ_{syn}	6 μ s / 10 μ s
input unit time constant	τ_{in}	8 μ s / -
input unit threshold	θ_{in}	0.2 / -
surrogate gradient steepness	β	50
learning rate	η	1.5×10^{-3}
learning rate decay (per epoch)	γ_η	0.03 / 0.025
burst regularization strength	ρ_b	0.05 / -
rate regularization strength	ρ_r	- / 0.6×10^{-3}
rate regularization threshold	θ_r	- / 600
time step/sample period	Δt	1.7 μ s
weight initialization spread	$\hat{\sigma}_w$	0.24

Acknowledgements

We express our gratitude towards O. Breitwieser, C. Mauch, E. Müller, and P. Spilger for their work on the software environment, B. Kindler, F. Kleveta, and S. Schmitt for their helpful support, A. Baumbach for his valuable feedback during the early commissioning phase of the system, and J. Göltz and L. Kriener for helpful discussions. We thank the whole Electronic Vision(s) group for the inspirational work environment.

This research has received funding from the European Union’s Horizon 2020 research and innovation programme under grant agreement Nos. 720270, 785907 and 945539 (Human Brain Project, HBP). This work was supported by the Novartis Research Foundation.

References

- D. H. Ackley, G. E. Hinton, and T. J. Sejnowski. A learning algorithm for boltzmann machines. *Cognitive science*, 9(1): 147–169, 1985.
- G. Bellec, D. Salaj, A. Subramoney, R. Legenstein, and W. Maass. Long short-term memory and learning-to-learn in networks of spiking neurons. In *Advances in Neural Information Processing Systems*, pages 787–797, 2018.
- Y. Bengio, N. Léonard, and A. Courville. Estimating or propagating gradients through stochastic neurons for conditional computation. *arXiv preprint arXiv:1308.3432*, 2013.
- B. V. Benjamin, P. Gao, E. McQuinn, S. Choudhary, A. R. Chandrasekaran, J.-M. Bussat, R. Alvarez-Icaza, J. V. Arthur, P. A. Merolla, and K. Boahen. Neurogrid: A mixed-analog-digital multichip system for large-scale neural simulations. *Proceedings of the IEEE*, 102(5):699–716, 2014.
- K. Boahen. A neuromorph’s prospectus. *Computing in Science & Engineering*, 19(2):14–28, 2017.
- S. M. Bohte. Error-backpropagation in networks of fractionally predictive spiking neurons. In *International Conference on Artificial Neural Networks*, pages 60–68. Springer, 2011.
- S. M. Bohte, J. N. Kok, and H. La Poutre. Error-backpropagation in temporally encoded networks of spiking neurons. *Neurocomputing*, 48(1):17–37, 2002.
- J. Brea, W. Senn, and J.-P. Pfister. Matching recall and storage in sequence learning with spiking neural networks. *Journal of neuroscience*, 33(23):9565–9575, 2013.
- T. B. Brown, B. Mann, N. Ryder, M. Subbiah, J. Kaplan, P. Dhariwal, A. Neelakantan, P. Shyam, G. Sastry, A. Askell, et al. Language models are few-shot learners. *arXiv preprint arXiv:2005.14165*, 2020.
- J. Büchel, D. Zendrikov, S. Solinas, G. Indiveri, and D. R. Muir. Supervised training of spiking neural networks for robust deployment on mixed-signal neuromorphic processors. *arXiv preprint arXiv:2102.06408*, 2021.
- G. K. Chen, R. Kumar, H. E. Sumbul, P. C. Knag, and R. K. Krishnamurthy. A 4096-neuron 1m-synapse 3.8-pj/sop spiking neural network with on-chip stdp learning and sparse weights in 10-nm finfet cmos. *IEEE Journal of Solid-State Circuits*, 54(4):992–1002, 2019.

- E. Chicca, F. Stefanini, C. Bartolozzi, and G. Indiveri. Neuro-morphic electronic circuits for building autonomous cognitive systems. *Proceedings of the IEEE*, 102(9):1367–1388, 2014.
- I. M. Comsa, T. Fischbacher, K. Potempa, A. Gesmundo, L. Versari, and J. Alakuijala. Temporal Coding in Spiking Neural Networks with Alpha Synaptic Function. In *ICASSP 2020 - 2020 IEEE International Conference on Acoustics, Speech and Signal Processing (ICASSP)*, pages 8529–8533, May 2020. doi: 10.1109/ICASSP40776.2020.9053856. ISSN: 2379-190X.
- M. Courbariaux, I. Hubara, D. Soudry, R. El-Yaniv, and Y. Bengio. Binarized neural networks: Training deep neural networks with weights and activations constrained to+ 1 or-1. *arXiv preprint arXiv:1602.02830*, 2016.
- B. Cramer, Y. Stradmann, J. Schemmel, and F. Zenke. The heidelberg spiking data sets for the systematic evaluation of spiking neural networks. *IEEE Transactions on Neural Networks and Learning Systems*, 2020.
- M. Davies. Benchmarks for progress in neuromorphic computing. *Nature Machine Intelligence*, 1(9):386–388, 2019.
- M. Davies, N. Srinivasa, T.-H. Lin, G. China, Y. Cao, S. H. Choday, G. Dimou, P. Joshi, N. Imam, S. Jain, et al. Loihi: A neuromorphic manycore processor with on-chip learning. *Ieee Micro*, 38(1):82–99, 2018.
- S. K. Esser, P. A. Merolla, J. V. Arthur, A. S. Cassidy, R. Appuswamy, A. Andreopoulos, D. J. Berg, J. L. McKinstry, T. Melano, D. R. Barch, and et al. Convolutional networks for fast, energy-efficient neuromorphic computing. *Proceedings of the National Academy of Sciences*, 113(41):11441–11446, Sep 2016. ISSN 1091-6490. doi: 10.1073/pnas.1604850113.
- C. Frenkel, M. Lefebvre, J.-D. Legat, and D. Bol. A 0.086-mm² 12.7-pj/sop 64k-synapse 256-neuron online-learning digital spiking neuromorphic processor in 28-nm cmos. *IEEE transactions on biomedical circuits and systems*, 13(1):145–158, 2018.
- S. Friedmann, J. Schemmel, A. Grübl, A. Hartel, M. Hock, and K. Meier. Demonstrating hybrid learning in a flexible neuromorphic hardware system. *IEEE Transactions on Biomedical Circuits and Systems*, 11(1):128–142, 2017. ISSN 1932-4545. doi: 10.1109/TBCAS.2016.2579164.
- S. Furber. Large-scale neuromorphic computing systems. *Journal of neural engineering*, 13(5):051001, 2016.
- B. Gardner and A. Grüning. Supervised learning in spiking neural networks for precise temporal encoding. *PloS one*, 11(8):e0161335, 2016.
- J. Göltz, A. Baumbach, S. Billaudelle, O. Breitwieser, D. Dold, L. Kriener, A. F. Kungl, W. Senn, J. Schemmel, K. Meier, et al. Fast and deep neuromorphic learning with time-to-first-spike coding. *arXiv preprint arXiv:1912.11443*, 2019.
- J. Guerguiev, T. P. Lillicrap, and B. A. Richards. Towards deep learning with segregated dendrites. *Elife*, 6:e22901, 2017.
- R. Gütiğ and H. Sompolinsky. The tempotron: a neuron that learns spike timing-based decisions. *Nat Neurosci*, 9(3):420–428, Mar. 2006. ISSN 1097-6256. doi: 10.1038/nn1643.
- K. He, X. Zhang, S. Ren, and J. Sun. Delving deep into rectifiers: Surpassing human-level performance on imagenet classification. In *Proceedings of the IEEE international conference on computer vision*, pages 1026–1034, 2015.
- D. Huh and T. J. Sejnowski. Gradient descent for spiking neural networks. In *Advances in Neural Information Processing Systems*, pages 1433–1443, 2018.
- E. Hunsberger and C. Eliasmith. Spiking deep networks with lif neurons. *arXiv preprint arXiv:1510.08829*, 2015.
- G. Indiveri, B. Linares-Barranco, T. J. Hamilton, A. Van Schaik, R. Etienne-Cummings, T. Delbruck, S.-C. Liu, P. Dudek, P. Häfliger, S. Renaud, et al. Neuromorphic silicon neuron circuits. *Frontiers in neuroscience*, 5:73, 2011.
- D. Jimenez Rezende and W. Gerstner. Stochastic variational learning in recurrent spiking networks. *Frontiers in Computational Neuroscience*, 8:38, 2014. ISSN 1662-5188. doi: 10.3389/fncom.2014.00038.
- D. P. Kingma and J. Ba. Adam: A method for stochastic optimization. *arXiv preprint arXiv:1412.6980*, 2014.
- Y. LeCun, L. Bottou, Y. Bengio, and P. Haffner. Gradient-based learning applied to document recognition. *Proceedings of the IEEE*, 86(11):2278–2324, 1998.
- J. H. Lee, T. Delbruck, and M. Pfeiffer. Training deep spiking neural networks using backpropagation. *Frontiers in neuroscience*, 10:508, 2016.
- C.-K. Lin, A. Wild, G. N. China, Y. Cao, M. Davies, D. M. Lavery, and H. Wang. Programming spiking neural networks on intel’s loihi. *Computer*, 51(3):52–61, 2018.
- M. Mahowald and R. Douglas. A silicon neuron. *Nature*, 354(6354):515–518, 1991.
- R.-M. Memmesheimer, R. Rubin, B. Ölveczky, and H. Sompolinsky. Learning Precisely Timed Spikes. *Neuron*, 82(4):925–938, May 2014. ISSN 0896-6273. doi: 10.1016/j.neuron.2014.03.026.
- P. A. Merolla, J. V. Arthur, R. Alvarez-Icaza, A. S. Cassidy, J. Sawada, F. Akopyan, B. L. Jackson, N. Imam, C. Guo, Y. Nakamura, et al. A million spiking-neuron integrated circuit with a scalable communication network and interface. *Science*, 345(6197):668–673, 2014.
- V. Mnih, K. Kavukcuoglu, D. Silver, A. Graves, I. Antonoglou, D. Wierstra, and M. Riedmiller. Playing atari with deep reinforcement learning. *arXiv preprint arXiv:1312.5602*, 2013.
- H. Mostafa. Supervised Learning Based on Temporal Coding in Spiking Neural Networks. *Trans Neural Netw Learn Syst*, 29(7):3227–3235, July 2018. doi: 10.1109/TNNLS.2017.2726060.
- M. Mozafari, M. Ganjtabesh, A. Nowzari-Dalini, and T. Masquelier. SpykeTorch: Efficient Simulation of Convolutional Spiking Neural Networks with at most one Spike per Neuron. *arXiv:1903.02440 [cs, q-bio]*, Mar. 2019. arXiv: 1903.02440.

- E. Müller, C. Mauch, P. Spilger, O. J. Breitwieser, J. Klähn, D. Stöckel, T. Wunderlich, and J. Schemmel. Extending brainscales os for brainscales-2. *arXiv preprint arXiv:2003.13750*, 2020.
- E. O. Neftci. Data and power efficient intelligence with neuromorphic learning machines. *iScience*, 5:52–68, 2018.
- E. O. Neftci, C. Augustine, S. Paul, and G. Detorakis. Event-driven random back-propagation: Enabling neuromorphic deep learning machines. *Frontiers in neuroscience*, 11:324, 2017.
- E. O. Neftci, H. Mostafa, and F. Zenke. Surrogate gradient learning in spiking neural networks: Bringing the power of gradient-based optimization to spiking neural networks. *IEEE Signal Processing Magazine*, 36(6):51–63, 2019.
- P. O’Connor and M. Welling. Deep spiking networks. *arXiv preprint arXiv:1602.08323*, 2016.
- A. Paszke, S. Gross, F. Massa, A. Lerer, J. Bradbury, G. Chanan, T. Killeen, Z. Lin, N. Gimelshein, L. Antiga, A. Desmaison, A. Kopf, E. Yang, Z. DeVito, M. Raison, A. Tejani, S. Chilamkurthy, B. Steiner, L. Fang, J. Bai, and S. Chintala. Pytorch: An imperative style, high-performance deep learning library. In H. Wallach, H. Larochelle, A. Beygelzimer, F. d’Alché Buc, E. Fox, and R. Garnett, editors, *Advances in Neural Information Processing Systems 32*, pages 8024–8035. Curran Associates, Inc., 2019.
- A. Payeur, J. Guerguiev, F. Zenke, B. Richards, and R. Naud. Burst-dependent synaptic plasticity can coordinate learning in hierarchical circuits. *bioRxiv*, 2020.
- M. Pfeiffer and T. Pfeil. Deep learning with spiking neurons: opportunities and challenges. *Frontiers in neuroscience*, 12:774, 2018.
- K. Roy, A. Jaiswal, and P. Panda. Towards spike-based machine intelligence with neuromorphic computing. *Nature*, 575(7784):607–617, 2019.
- B. Rückauer, N. Känzig, S.-C. Liu, T. Delbruck, and Y. Sandomirskaya. Closing the accuracy gap in an event-based visual recognition task. *arXiv preprint arXiv:1906.08859*, 2019.
- J. Schemmel, D. Brüderle, A. Grübl, M. Hock, K. Meier, and S. Millner. A wafer-scale neuromorphic hardware system for large-scale neural modeling. *Proceedings of the 2010 IEEE International Symposium on Circuits and Systems (ISCAS’10)*, pages 1947–1950, 2010.
- S. Schmitt, J. Klähn, G. Bellec, A. Grübl, M. Guettler, A. Hartel, S. Hartmann, D. Husmann, K. Husmann, S. Jeltsch, et al. Neuromorphic hardware in the loop: Training a deep spiking network on the brainscales wafer-scale system. In *2017 International Joint Conference on Neural Networks (IJCNN)*, pages 2227–2234. IEEE, 2017.
- S. B. Shrestha and G. Orchard. Slayer: Spike layer error reassignment in time. In *Advances in Neural Information Processing Systems*, pages 1412–1421, 2018.
- D. Silver, J. Schrittwieser, K. Simonyan, I. Antonoglou, A. Huang, A. Guez, T. Hubert, L. Baker, M. Lai, A. Bolton, et al. Mastering the game of go without human knowledge. *nature*, 550(7676):354–359, 2017.
- P. Sterling and S. Laughlin. *Principles of neural design*. MIT Press, 2015.
- C. Stöckl and W. Maass. Classifying images with few spikes per neuron. *arXiv preprint arXiv:2002.00860*, 2020.
- E. Stomatias, D. Neil, M. Pfeiffer, F. Galluppi, S. B. Furber, and S.-C. Liu. Robustness of spiking deep belief networks to noise and reduced bit precision of neuro-inspired hardware platforms. *Frontiers in Neuroscience*, 9:222, 2015. ISSN 1662-453X. doi: 10.3389/fnins.2015.00222.
- A. Tavanaei, M. Ghodrati, S. R. Kheradpisheh, T. Masquelier, and A. Maida. Deep learning in spiking neural networks. *Neural Networks*, 111:47–63, 2019.
- S. Wozniak, A. Pantazi, and E. Eleftheriou. Deep Networks Incorporating Spiking Neural Dynamics. *arXiv:1812.07040 [cs]*, Dec. 2018.
- B. Yin, F. Corradi, and S. M. Bohtë. Effective and efficient computation with multiple-timescale spiking recurrent neural networks. *arXiv preprint arXiv:2005.11633*, 2020.
- S. Yin, S. K. Venkataramanaiah, G. K. Chen, R. Krishnamurthy, Y. Cao, C. Chakrabarti, and J.-s. Seo. Algorithm and hardware design of discrete-time spiking neural networks based on back propagation with binary activations. In *2017 IEEE Biomedical Circuits and Systems Conference (BioCAS)*, pages 1–5. IEEE, 2017.
- D. Zambrano, R. Nusselder, H. S. Scholte, and S. M. Bohtë. Sparse computation in adaptive spiking neural networks. *Frontiers in neuroscience*, 12:987, 2019.
- F. Zenke and S. Ganguli. Superspike: Supervised learning in multilayer spiking neural networks. *Neural computation*, 30(6):1514–1541, 2018.